Separating particles according to their physical properties: Transverse drift of underdamped and overdamped interacting particles diffusing through two-dimensional ratchets

Sergey Savel'ev,[1] Vyacheslav Misko,[1,2] Fabio Marchesoni,[1,3] and Franco Nori[1,2]
[1]*Frontier Research System, The Institute of Physical and Chemical Research (RIKEN), Wako-shi, Saitama, 351-0198, Japan*
[2]*Center for Theoretical Physics, Center for the Study of Complex Systems, Department of Physics, University of Michigan, Ann Arbor, Michigan 48109-1120, USA*
[3]*Dipartimento di Fisica, Universitá di Camerino, I-62032 Camerino, Italy*
(Received 15 September 2004; revised manuscript received 3 January 2005; published 27 June 2005)

We study the transverse net current of particles moving through two-dimensional (2D) square arrays or chains of potential energy hills or wells when driven perpendicularly to their spatial symmetry axis (i.e., the mirror-symmetry axis). This transverse rectification is quite general and occurs for nonzero inertia, and/or interaction, and/or temperature. We separately consider both cases: underdamped and overdamped interacting particles. The interplay between inertia and thermal fluctuations, no matter how weak, determines robust rectification properties, that allow distinct control techniques for transport of underdamped (e.g., electrons or colloids) versus overdamped particles (e.g., vortices) in asymmetric nanodevices and microdevices. Furthermore, the transverse rectification of interacting particles moving through 2D asymmetric potential landscapes can drop to zero if their interaction length is smaller than a certain characteristic geometric length. This size-selective rectification mechanism could be used for developing particle separation devices.

DOI: 10.1103/PhysRevB.71.214303 PACS number(s): 82.70.−y, 05.40.−a, 05.60.Cd

I. INTRODUCTION

The motion of small particles through different types of asymmetric potential landscapes has become a growing topic leading to different types of microdevices and nanodevices.[1–17] Also, these might provide a deeper understanding of several biological systems (e.g., ion-channel transport[18,19] in cell membranes). A way of controlling the motion of tiny particles[20] moving on an asymmetric substrate is to apply an unbiased stochastic force or an alternating drive that induce a net particle drift (the so-called ratchet or rectification effect.[2]) Although this general mechanism seems to be applicable to any type of particles (including electrons, colloidal particles, vortices in superconductors, etc.), inertia effects and interparticle interactions can strongly affect the rectification.

However, most cases studied so far[2] are restricted to one-dimensional (1D) motion of either overdamped particles in the presence of noise (finite temperature) or deterministic (noiseless) underdamped/interacting particles. For instance, it was found (see, e.g., Refs. 21 and 22) that deterministic 1D inertial ratchets exhibit a complicated irregular behavior which is extremely sensitive to changing parameters and initial conditions owing to the presence of numerous competing dynamical attractors (both chaotic and periodic). Such underdamped noiseless ratchets are of little use for the operation of reliable devices because of their very unpredictable transport properties. Also, it is not clear how experimentally unavoidable noise (temporal or spatial) can influence the complicated behavior of these deterministic 1D ratchets.

Here, we compare the underdamped *and* overdamped dynamics associated with, e.g., electrons in ballistic regimes, dilute charged colloids and vortices in superconductors. We have found that the interplay between temperature and inertia can lead to robust features of the net current, which are absent in both overdamped (noisy) and deterministic (noiseless) two-dimensional (2D) ratchets. The regular characteristics of this class of ratchets is due to the fact that adding any level of noise to the system amounts to averaging over the many dynamical attractors that govern its response.

Even though 1D models describe a wide variety of different physical systems,[2,16,23] including colloids in arrays of optical tweezers,[7] interacting binary mixtures driven on (asymmetric) periodic substrates,[24–26] ferrofluids,[27] etc., there are some two-dimensional and three-dimensional problems which are hardly reducible to the 1D case and exhibit very unusual behaviors (e.g., Ref. 28). Here we study one of these irreducible problems when particles are driven on an asymmetric *two-dimensional* potential landscape by an ac or dc driving force perpendicularly to the symmetry axis of the potential (Fig. 1). Such a geometry has recently attracted broad interest[29–38] in the context of separation of macromolecules, DNA, or even cells, because the induced transverse drift separates different objects depending on their self-diffusion constant D. We conclude that *even relatively weak inertial effects and interparticle interactions can strongly affect the transverse current*, especially at low temperatures. This could be used to separate different objects with respect to not only diffusion but also their mass, interaction constant (say, charge or magnetic moment) or even interaction length.

Examples of landscapes sustaining transverse rectification are: asymmetric potential hills or wells, forming 1D chains or 2D lattices made of such potentials. Inspired by recent experiments performed for both electrons[14,15] and vortices,[12] we use potential hills/wells with triangular cross section as a unit of the potential landscapes. It is easy to prove that for these geometries (see, e.g., Fig. 1) an overdamped particle (ac or dc) driven perpendicularly to the symmetry axis has

TABLE I. Brief summary of some of the results obtained in this work.

Rectification induced by	Diffusion, Sec. III	Inertia, Sec. IV		Interaction, Sec. V
	Hills, wells	Hills	Wells	Hills
Type of motion	Noisy (Fig. 2)	Periodic attractors (closed trajectories), Figs. 3(c) and 3(d)	Chaotic (irregular), Figs. 4(c)–4(e)	Either periodic or chaotic, Figs. 5(b)–5(e) Latticelike structure at low drives [Fig. 5(b)] for long-range strong interaction
Influence of vertical gaps between pyramids	Minor	Minor	For $T=0$, a very small gap suppresses rectification (Fig. 4, up triangles)	Zero rectification for $\lambda < \lambda_c$ [Fig. 6(a)]
Interplay with temperature		Averaging over many periodic attractors [Fig. 3(e)]; smoothing the $\langle V(A_0)\rangle$ curve makes rectification more controllable [Fig. 3(a), red solid circles]	Restores rectification for nonzero vertical gap [Fig. 4(b), solid squares]	Smooth $\langle V(A_0)\rangle$ curve; $\langle V(A_0)\rangle$ for short-range weak and long-range strong interactions become similar
Dependence on driving amplitude	Smooth [Fig. 2(c)]	For $T=0$, very sharp, irregular $\langle V(A_0)\rangle$ is nonzero within several amplitude intervals [Fig. 3(a), open circles; Fig. 3(b)] corresponding to different winding numbers; at $T\neq 0$, $\langle V(A_0)\rangle$ is smooth with a pronounced peak [Fig. 3(a), solid circles]	Sharp cutoff in $\langle V(A_0)\rangle$ dependence at small A_0, plateau for relatively large A_0 interval [Fig. 4(a)]	For $T=0$ smooth; cut off at small A_0 [Fig. 5(a)]. A longer tail at large drives for long-range strong interaction

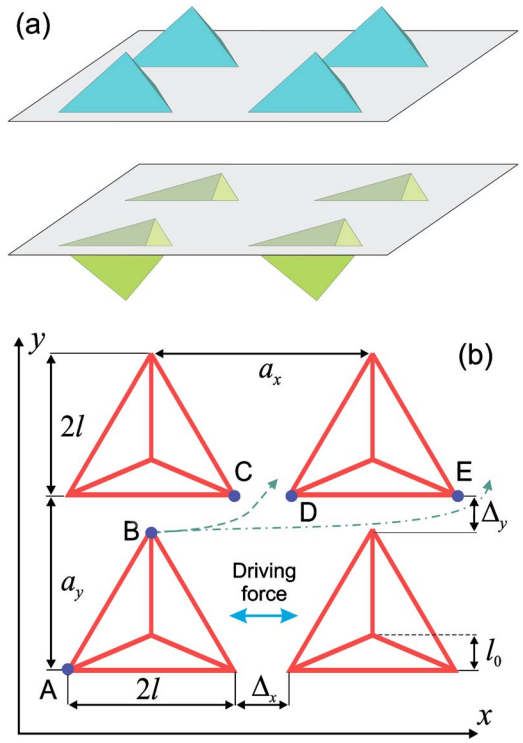

FIG. 1. Asymmetric 2D arrays of potential energy hills [top of (a)] and potential wells [bottom of (a)]: (a) side view; (b) top view. The parameters l, l_0, a_x, a_y, Δ_x, Δ_y define the geometry of the array. The dashed and dash-dotted arrows starting at point B show two typical trajectories of a rectified particle (see Appendix A). The blue dots denote specific corners which are used in the text to describe particle motion around the triangles.

zero net velocity in the absence of noise, i.e., at zero temperature, $T=0$. Indeed, sooner or later each particle gets captured in a horizontal lane between two triangle rows and then keeps oscillating back and forth in it forever. However, at finite temperature, fluctuations push the particle out of its lane, thus inducing a net transverse current.[38] Therefore, *diffusion plays a key role in the 2D rectifiers studied here*, as was also found, e.g., with the asymmetric vortex channels of Ref. 39. Similarly, even though inertia and particle interactions are often ignored in ratchet-related studies, these factors are indeed crucial in our work and can sustain rectification even at or near zero temperature.

The main goal of this paper is to show *how inertia and particle-particle interaction cause transverse rectification in 2D potentials* and how these results are affected by temperature. Results obtained here could be used for improving existing separation techniques[29–38,40] and for future implementations of spin/charge/mass separation of particles. The summary of the results obtained here is presented in Table I.

II. MODEL

The dynamics of an assembly of particles of mass m moving on an asymmetric 2D potential

$$U(x,y)=\sum_{k_x,k_y=-\infty}^{\infty} U_e(x-a_xk_x,y-a_yk_y), \tag{1}$$

can be described by the Langevin equations

$$m\ddot{x}_i=-\eta\dot{x}_i-\frac{\partial U(x_i,y_i)}{\partial x_i}+A(t)-\sum_{j\neq i}\frac{\partial W(x_i-x_j,y_i-y_j)}{\partial x_i}+\sqrt{2\eta T}\xi_x^{(i)}(t),$$

$$m\ddot{y}_i=-\eta\dot{y}_i-\frac{\partial U(x_i,y_i)}{\partial y_i}-\sum_{j\neq i}\frac{\partial W(x_i-x_j,y_i-y_j)}{\partial y_i}+\sqrt{2\eta T}\xi_y^{(i)}(t). \tag{2}$$

In contrast to other 2D overdamped systems,[12,16,39,41,42] the problem considered here is harder to simulate and more CPU-time consuming. Without loss of generality, we simulated these equations for a potential landscape made of elementary pyramidal[43] blocks $U_e(x,y)$:

$$U_e=\frac{q(y+l)}{l_0}$$

if $-l<x\leqslant 0$, $-l<y<l_0(x+l)/l-l$, and $0<x<l$, $-l<y<-l_0(x-l)/l-l$;

$$U_e=\frac{q(2x+l-y)}{(2l-l_0)}$$

if $-l<x<0$, $l_0(x+l)/l-l<y<2x+l$; and

$$U_e=\frac{q(l-2x-y)}{(2l-l_0)}$$

if $0<x<l$, $-l_0(x-l)/l-l<y<l-2x$.

This potential block is chosen just as a specific example of an asymmetric 2D potential. Figure 1 illustrates a square array of these pyramids for potential hills, $q>0$, and for potential wells, $q<0$. Unlike previous works using 2D triangular traps,[12,16,41,42] the potential studied here has two types of asymmetry: the triangular shape of its building blocks and the asymmetry associated with the "internal" (pyramidal) structure of each block, controlled by the elongation parameter l_0. The latter asymmetry affects the motion of the particles only if the drive is strong enough to push them across the obstacles/traps. The intensity of the white noise is proportional to the square root of the temperature T and of the viscosity η, with correlation functions $\langle\xi_\alpha^{(i)}\rangle=0$ and $\langle\xi_\alpha^{(i)}(t)\xi_\beta^{(j)}(0)\rangle=\delta(t)\delta_{ij}\delta_{\alpha\beta}$. Here α, $\beta=x$ or y, where i, j are particle labels, and δ denotes either a delta-function $\delta(t)$ or a Kronecker symbol $\delta_{\alpha\beta}$. For the pair interaction potential W, we use a cutoff logarithmic function with interaction constant g, namely

$$W=gr_{i,j}$$

for $r_{i,j}=\sqrt{(x_i-x_j)^2+(y_i-y_j)^2}<\lambda_{\min}$,

$$W=g\lambda_{\min}\left[\ln\left(\frac{r_{i,j}}{\lambda_{\min}}\right)+1\right]$$

for $\lambda_{\min}<r_{i,j}<\lambda$, and zero otherwise. A force

$$A(t)=A_0\mathrm{sgn}[\cos(2\pi\nu t)]$$

(with amplitude A_0 and frequency ν; $\nu=0$ corresponds to a dc drive A_0) applied along the x axis, i.e., perpendicular to

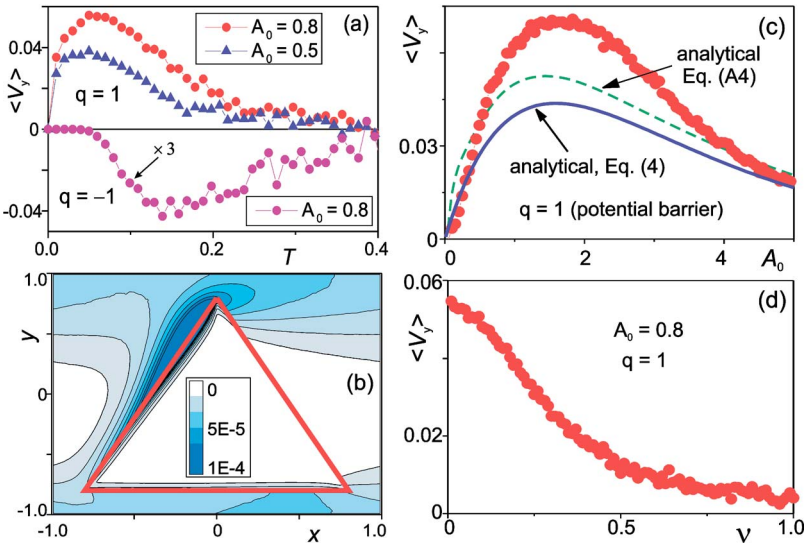

FIG. 2. (Color online) (a) Diffusion-induced transverse net velocity $\langle V_y \rangle$ vs temperature T for massless and noninteracting particles moving through the 2D array of triangles shown in Fig. 1 Parameters are: $q=1$ for a potential hill, $q=-1$ (where the net velocity is magnified by a factor of 3) for a potential well, $a_y=a_x=2$, $l=0.8$ (i.e., $\Delta_x=\Delta_y=0.4$), and $\eta=1$. (b) The contour plot of the particle distribution $f(x,y)$ around a potential hill at $T=0.06$; all remaining parameters are as in (a). $\langle V_y \rangle$ vs amplitude A_0 [(c) red circles)] and frequency ν (d) of the ac driving force $A(t)$. Here parameters are as in (c). Blue solid (green dashed) line in (c) is the estimated net velocity in Eq. (4) [Eq. (A4)].

the symmetry axis, induces a particle drift in the y direction. This is the *transverse rectification* effect we investigated in detail. In order to integrate Eqs. (2) we employ the Euler method. The time step used is $\Delta t \lesssim 0.0013$, and we usually perform $\gtrsim 10^7$ steps, depending on the rate of convergence and on whether an ac or dc signal is applied. We have also used different interaction potentials, including $W=g(\lambda-r_{i,j})$ for $r_{i,j}<\lambda$, and 0 otherwise as well as the vortex-vortex-interaction-potential $W=g\lambda^2\exp(-r_{i,j}/\lambda)/r_{i,j}$, and have found that our results do not qualitatively depend on the specific form of the interaction, as long as the interactions are repulsive.

When the interaction constant g is zero (i.e., when transverse rectification is induced via diffusion and/or inertia), particles moving in different potential cells (corresponding to different values of k_x and k_y) do not interact with one another. Therefore, there is no need to impose any additional boundary conditions. For interacting particles $g \neq 0$, we assume periodic boundary conditions within a simulation cell containing many ($\geqslant 9$) lattice cells. The linear size ($\sim 10\lambda$) of this cell has been chosen to be much larger than the interaction length λ.

The 2D particle distribution densities $f(x,y)$ discussed in the following sections, are defined as:

$$f(x,y) = \left\langle \sum_i \delta[x - x_i(t)]\delta[y - y_i(t)] \right\rangle_t \tag{3}$$

with the average $\langle \ldots \rangle_t$ taken over the time of a simulation run.

III. DIFFUSION-INDUCED TRANSVERSE RECTIFICATION

The case of massless ($m=0$) and non-interacting particles ($g=0$) has been studied at length in the earlier literature (e.g., Refs. 29–38). However, in contrast to all previous works, we solved numerically the Langevin Eqs. (2) without any additional simplification and studied both potential hills ($q>0$) and wells ($q<0$). Our results are shown in Fig. 2(a): the transverse net velocity $\langle V_y \rangle$ attains a maximum at low temperatures for both $q>0$ and $q<0$. The dependence of $\langle V_y \rangle$ on the driving amplitude A_0 also shows a maximum [Fig. 2(c)], so that the net current can be tuned to a desired value within an appropriate range. Increasing the frequency gradually reduces the rectification effect [Fig. 2(d)].

The mechanism of transverse rectification can be understood as follows. Let us consider for instance the case of repelling barriers with $q>0$ (the case of attractive potential wells $q<0$ can be interpreted in a similar way). When the driving force along the x direction pushes (from left to right) the particles against the left side of a pyramid, the particle distribution tends to accumulate near the tip [darker regions Fig. 2(b)] of its triangular basis [point B in Fig. 1(b)]. Then, the particles diffuse into the horizontal lane behind it and across the row of pyramids just above it [e.g., between points B and C in Fig. 1(b)]. Using this physical picture, one can easily obtain an approximate equation for the transverse velocity $\langle V_y \rangle$ (see Appendix A):

$$\langle V_y \rangle = \frac{A_0 P_{\mathrm{diff}}}{\eta(a_x + 4l)},$$

$$P_{\mathrm{diff}} = \frac{1}{2} - \frac{1}{2\sqrt{\pi}} \int_{-\infty}^{\infty} dz \exp(-z^2)\Phi[\alpha(z-\beta)]. \tag{4}$$

Here, we introduced the error function

$$\Phi(x) = \frac{2}{\sqrt{\pi}} \int_0^x dz \exp(-z^2)$$

and the combined parameters

$$\alpha = \sqrt{\frac{l}{\Delta_x}}, \quad \beta = \frac{\Delta_y}{2}\sqrt{\frac{A_0}{Tl}}$$

with

$$\Delta_y \equiv a_y - 2l, \quad \Delta_x \equiv a_x - 2l.$$

In the limit of large spacing between triangles along the x direction, $\alpha \to 0$, the probability for a particle to diffuse one pyramid row along the y direction, P_{diff}, approaches $1/2$.

Comparing the analytical prediction in Eq. (4) [Fig. 2(c), solid line] with our simulation results [Fig. 2(c), solid circles], one can see that the agreement is qualitative, as we underestimate the peak of the net velocity curve. This discrepancy seems to be related to the fact, ignored in Eq. (4), that two adjacent horizontal lanes are connected by more than one opening. In other words, particles impinging on the triangle side AB are pushed into the lane behind point B [see Fig. 1(b)]: some of them can diffuse then into the lane above it across the opening between points C and D (dashed trajectory), as accounted for in Eq. (4), while others do it through the openings lying farther to the left of E (e.g., dash-dotted trajectory). Simple estimates [Appendix A and Eq. (A4)] for the net velocity—when successfully diffusing through (e.g., five) other openings—provide a better agreement with our simulation data [see Fig. 2(c), green dashed line].

IV. TRANSVERSE CURRENT OF UNDERDAMPED PARTICLES

The case studied in the previous section applies only to massless noninteracting particles, e.g., magnetic flux quanta in superconductors at very low magnetic fields. However, for some colloidal particles inertia can become important. Moreover, inertial effects dominate over thermal fluctuations in ballistic electron rectifiers[14,15] and have been recently explored experimentally with vortices in asymmetric potentials.[44] In this section, we discuss how inertia affects the transverse rectification by setting $g=0$ and $m \neq 0$; we consider both the noiseless case $T=0$ and the low temperature limit $T \ll q$.

In order to make inertial effects more pronounced, we first consider a potential landscape where triangles (i.e., the pyramid bases) are stacked vertically with the tip of one touching the base of the triangle right above (i.e., $\Delta_y = 0$), while horizontally well spaced (i.e., $\Delta_x \neq 0$). Namely, the triangles are arranged to form vertical chains that run parallel to one another a distance Δ_x apart. The case of a single triangle chain, with particles being ac driven perpendicularly to it, is a particular case of this geometry. In view of experimental applications, we note that this geometry can mimic asymmetric membranes [see inset to Fig. 3(b)]. Note also that such a simple model of a membrane is much easier to manufacture since there is no need to keep the same spacings between triangles along the x direction. Moreover, slight variations (due to fabrication limitations) of the triangle length along the y direction do not significantly affect the performance of the membrane.

We concentrate here on the case of moderate masses, when inertia suffices to couple the motion along the x and y directions, but the velocity relaxes to its stationary value A/η between two subsequent particle-triangle collisions. In order to determine the region of parameters in which the approximation of moderate mass is valid, we assume that the characteristic time scale of the problem is m/η, while the characteristic force (for optimal rectification) is q/l; hence, the characteristic length $\delta = mq/\eta^2 l$. Relaxation of the particle trajectories between two successive collisions requires that $\delta \ll \Delta_x$, i.e.,

$$\Delta_x \gg \frac{qm}{\eta^2 l}.$$

In this regime, the transverse motion of the particles is robust with respect to noise and occurs for both ac and dc drives.

Rectification mechanism for potential hills and wells

In contrast to the usual diffusion-induced rectification, the rectification mechanism considered here ($m \neq 0, g=0$) is completely different for the case of potential hills and wells [see Figs. 3(a), 3(b), 4(a), and 4(b)]. In the case of potential hills, $q>0$, and zero noise, $T=0$, the dependence of the transverse velocity on the dc drive shows several amplitude windows with a nonzero net current corresponding to closed trajectories [periodic dynamical attractors, Fig. 3(c)] with well defined winding numbers N (i.e., numbers of cells a particle crosses along the x direction in order to advance by one cell in the y direction), as shown in Fig. 3(a). By changing initial conditions, we have found that the basins of these attractors are rather large. If an ac drive is applied, then an additional condition—trajectory locking when the drive changes sign [Fig. 3(d)]—has to be satisfied for a periodic transverse motion to set in. This results in the splitting of the amplitude regions corresponding to a nonzero transverse velocity at $\nu=0$ (dc force), into narrower-A_0 subregions corresponding to nonzero net velocities for $\nu>0$ [ac force, see Fig. 3(b)]. An example of closed trajectories for ac drives is shown in Fig. 3(d). Therefore, the rectangular-stepwise dependence of $\langle V_y \rangle$ on A_0 for the ac case [Fig. 3(b)] substantially differs from the dc case [Fig. 3(a)].

Even a small amount of noise, $T \ll q$, makes a huge impact on rectification: *transverse velocities for dc ($\nu=0$) and ac ($\nu=0.01$) drives coincide* within the accuracy of our simulation—while differing dramatically for $m=0$ and $T=0$ [see Figs. 3(a) and 3(b)]. This happens because stochastic averages over noise imply averaging over different dynamical attractors, namely over the corresponding deterministic trajectories [see Fig. 3(e)]. At finite temperatures, $\langle V_y \rangle$ exhibits an apparent smooth peak in that amplitude range where a rectangular-stepwise dependence is found for zero noise rectification. Thus, a constructive interplay of inertial dynamics and thermal fluctuations is observed, at variance with the 1D cases studied so far (see, e.g., Ref. 22). In other words, even a very weak thermal noise smears out many narrow-A intervals of either zero or large rectification into a smooth continuous curve [Fig. 3(a)]. This makes the rectification well-controlled and, thus, potentially useful for applications. Also, a well-pronounced maximum in the $\langle V_y(A_0) \rangle$ dependence could allow to separate particles according to their mass.

For the case of potential wells, $q<0$, we have found no periodic (closed) trajectories for moderate inertia (m

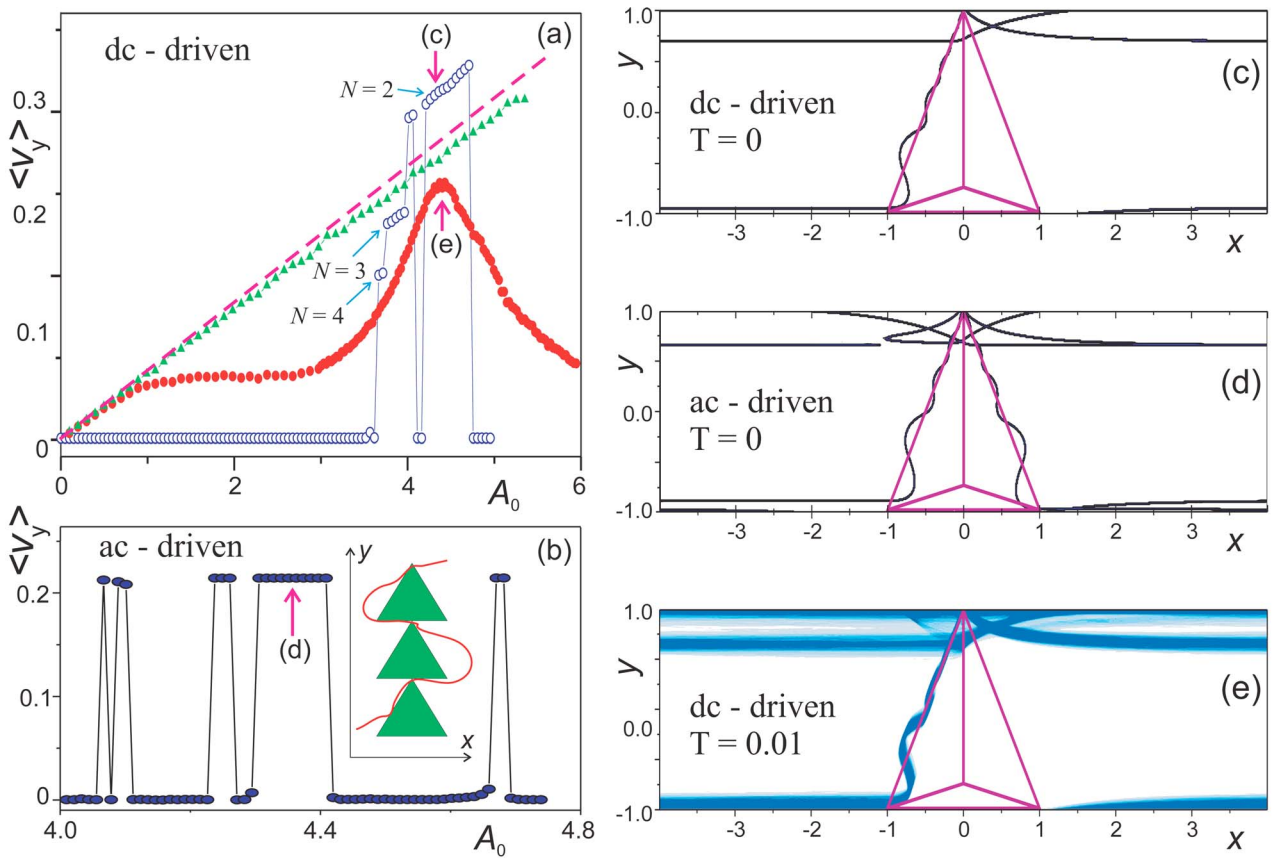

FIG. 3. (Color online) Transverse net velocity $\langle V_y \rangle$ of underdamped noninteracting massive particles ($m=0.8$, $\eta=2$, and $g=0$) driven by a dc (a) or an ac force (b) through an array of vertically arranged chains of pyramidal-shaped potential energy barriers ($q=8, l=1, a_y=2, a_x=8, \Delta_y=0, \Delta_x=6$); initial conditions are $x(t=0)=-4$, $y(0)=-0.9$, $v_x(0)=v_y(0)=0$. Panel (a): blue open circles/red solid circles correspond to the deterministic ($T=0$) and a weak noise ($T=0.01$) case, respectively; the slanted steps of $\langle V_y(A_0) \rangle$ at $T=0$ correspond to trajectory winding numbers $N=4$, 3, 2; green solid triangles represent the overdamped massless case ($T=0.01, m=0$), shown for comparison, together with the corresponding analytical estimate [Eq. (4) for $P_{\mathrm{diff}}=1/2$] drawn as a pink dashed straight line. Panel (b): The net transverse velocity as a function of the amplitude A_0 for an ac-drive of the deterministic massive case $T=0$, $m=0.8$, $\nu=0.051$. The inset schematically shows a trajectory of the rectified ac particle motion through a chain (membrane) of triangular potential hills. Panels (c),(d): Particle distributions for dc and ac drives ($\nu=0.051$), respectively, and same amplitude $A_0=4.5$; the existence of periodic deterministic trajectories is apparent. Panel (e): Particle distribution for temperature $T=0.01$ and a dc drive. The trajectories in (c)-(d) are stable against weak thermal fluctuations with $T=0.01$. As a result, at low frequency and finite temperature (here $T=0.01$), the curves $\langle V_y(A_0) \rangle$ are insensitive to ν, i.e., the ac and dc cases coincide within simulation accuracy.

$=0.8, \gamma=2$). Instead, a highly irregular ("chaotic") motion occurs [Fig. 4(c)]. This apparently ergodic behavior allows particles to cross the horizontal lanes delimited by triangle rows (somewhat similar to the case with thermal noise) thus inducing transverse rectification [Fig. 4(a), red open squares]. This very irregular particle motion agrees with our finding that dc and low-frequency ac drives produce the same net velocity within the accuracy of our simulations [both shown by open red squares in Fig. 4(a)].

Let us now consider the case of a finite vertical spacing between triangles, $\Delta_y > 0$. In contrast to the closed trajectory case (Fig. 4), a very small gap between triangles completely suppresses rectification [Fig. 4(b), green triangles]. This indicates that particles are densely distributed in space with a finite probability to get trapped into a narrow horizontal lane between triangle rows. Eventually, particles end up moving along one of these lanes and rectification drops to zero. Thermal fluctuations, no matter how low the temperature, prevent such a trajectory confinement and restore transverse rectification [Fig. 4(a), solid curve; Fig. 4(b), red and blue squares]. Particle distributions for small Δ_y and low temperatures are similar to those for $\Delta_y=0$ and $T=0$ but are markedly different from the distributions of massless (overdamped) particles—compare Figs. 4(c)–4(e) and Fig. 2(b). This demonstrates that the particle motion is still governed by the deterministic chaotic dynamics despite the stochastic average imposed by the presence of noise. Note that a particle spends inside a triangle an average time

$$\tau = \frac{l\eta}{A_0}.$$

Thus, its momentum change (momentum transfer from the x to the y direction) per collision is

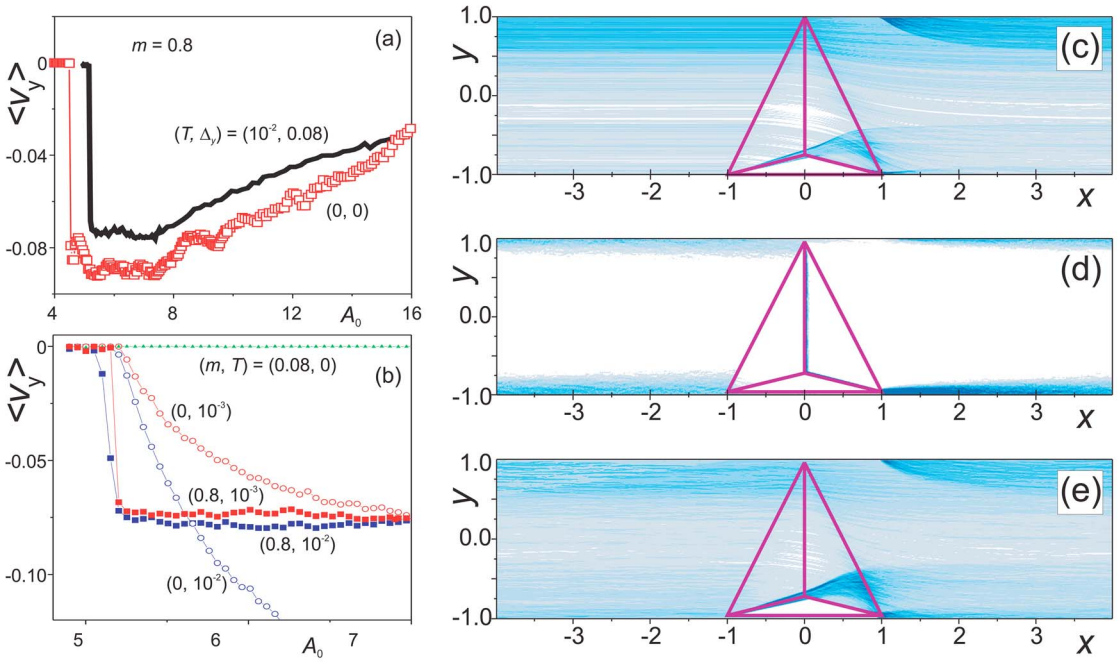

FIG. 4. (Color online) Transverse net velocity $\langle V_y \rangle$ vs amplitude A_0 for underdamped [$m=0.8$, $\eta=2$, in (a), (b)] and overdamped [$m=0$, $\eta=2$, in (b)] particles moving through a chain ($a_y=2$, $a_x=8$, $\Delta_x=6$, $\Delta_y=0$ (c), $\Delta_y=0.08$ (d), (e)] of tetragonal potential wells $q=-5$. In (b) $\langle V_y \rangle$ is displayed vs A_0 for different m and T. Even though the net transverse current at $T=0$ is non-zero for zero gap $\Delta_y=0$ [see (a)], $\langle V_y \rangle$ drops to zero for $\Delta_y>0$ if $T=0$. This is because the chaotic (i.e., irregular) motion (c) results in a finite probability for particles to be captured in-between triangles. Very weak temperatures almost recover the original distribution for gapless chains of triangles [compare (c) for $\Delta_y=0$, $T=0$, and (e) for $\Delta_y=0.08$, $T=0.01$] which is very different from the overdamped distribution in (d). All distributions shown here use the same parameters as in (a) and (b), and $A_0=5.3$.

$$\Delta P \sim \frac{\tau q}{l} \sim \frac{q\eta}{A_0}.$$

However, the number of collisions per unit time N_c increases linearly with the velocity of the particle, $N_c \sim A_0/\eta a_x$. Therefore, its momentum change per unit time $\tilde{P}$ turns out to be independent of A_0, that is

$$\tilde{P} = N_c \Delta P \sim \frac{q}{a_x}.$$

This explains the plateaus of the curves $\langle V_y(A_0) \rangle$ for $m=0.8$ displayed in Fig. 4(b).

Finally, let us consider the opposite limit: a particle with very large mass, $a_x \ll qm/(\eta^2 l)$. In this limit, the particle can change its trajectory only slightly during a single triangle-particle collision. As a consequence, transverse net motion does take place when a dc drive is applied along the x axis (see Appendix B), but this motion looks unstable with respect to temperature and could not be confirmed for ac forces, either.

V. TRANSVERSE MOTION OF OVERDAMPED INTERACTING PARTICLES

As discussed in Sec. III, thermal noise suffices to induce transverse motion of driven massless particles in the geometries considered here. However, interaction among particles also contributes to transverse rectification and can play a dominant role if the interaction constant, or the particle density are large enough. For instance, for vortices in asymmetric arrays (see, e.g., Ref. 12), diffusion can be important only if the magnetic field is slightly higher than the first critical magnetic field. At higher magnetic fields, rectification of magnetic flux quanta is controlled by the intervortex interactions, which lead to a current inversion[12] when vortices are driven along the y axis. Here, we show how interaction controls transverse rectification for both weak short-range and strong long-range interparticle forces. These two cases are studied in order to compare colloidal particles versus vortices, or vortices at low temperatures versus vortices at high temperatures. Taking $m=0$, and $g \neq 0$ in Eq. (2), we consider chains of triangles with $\Delta_y=0$, as well as 2D square arrays of potential hills with $\Delta_y>0$ and $\Delta_x>0$.

Let us first consider our chains of pyramidal obstacles, $q>0$. Even though the particle interactions have a strong impact on the equilibrium particle distribution—with a transition from a disordered liquidlike to an ordered latticelike phase [Figs. 5(b)–5(e)]—the transverse current $\langle V_y \rangle$ shows a qualitatively similar A_0 dependence for both weak short-range and strong long-range interactions. Namely, $\langle V_y(A_0) \rangle$ attains a maximum when $A \sim q/l$. However, the curves $\langle V_y \rangle$ vs A_0 exhibit longer tails for strong long-range interactions [see Fig. 5(a)]. The region of the linear growth of $\langle V_y \rangle$ for both the long-range strong and short-range weak interactions corresponds to the regime when a constant fraction of par-

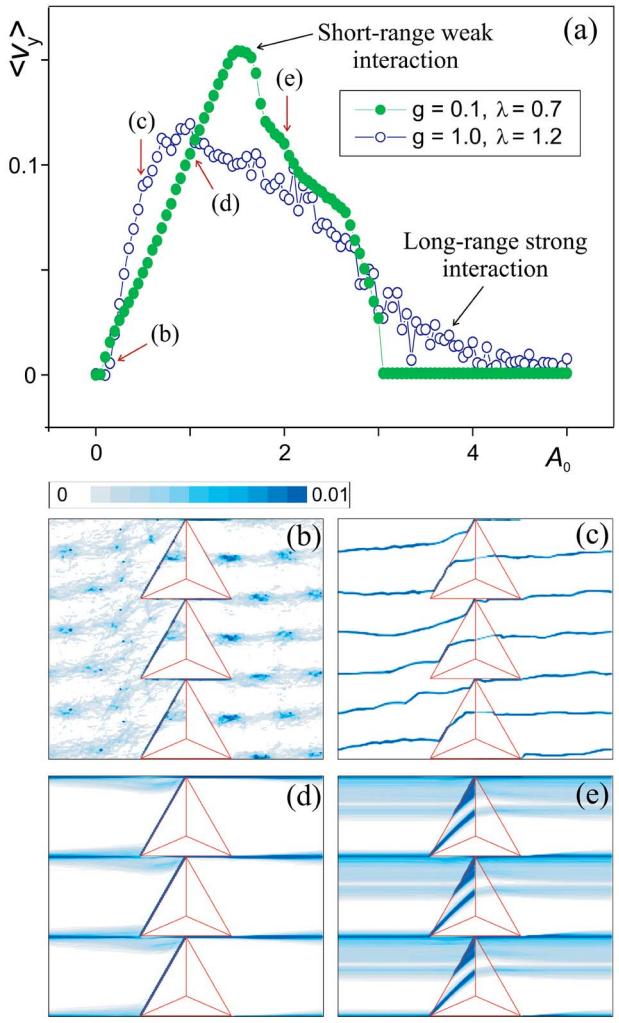

FIG. 5. (Color online) (a) Transverse net velocity $\langle V_y \rangle$ vs A_0 for interacting particles ac driven through a gapless triangular chain: $m=0$, $a_y=2$, $a_x=6$, $l=1$, $\Delta_x=4$, $\Delta_y=0$, $q=1$, $\lambda_{\min}=0.05$, and $T=0$. Green solid circles are for weak short-range interacting particles, while blue open circles are for strong long-range interacting particles. Particle distributions for strong long-range (b), (c) and weak short-range (d), (e) interactions for the A_0 values indicated by arrows in (a).

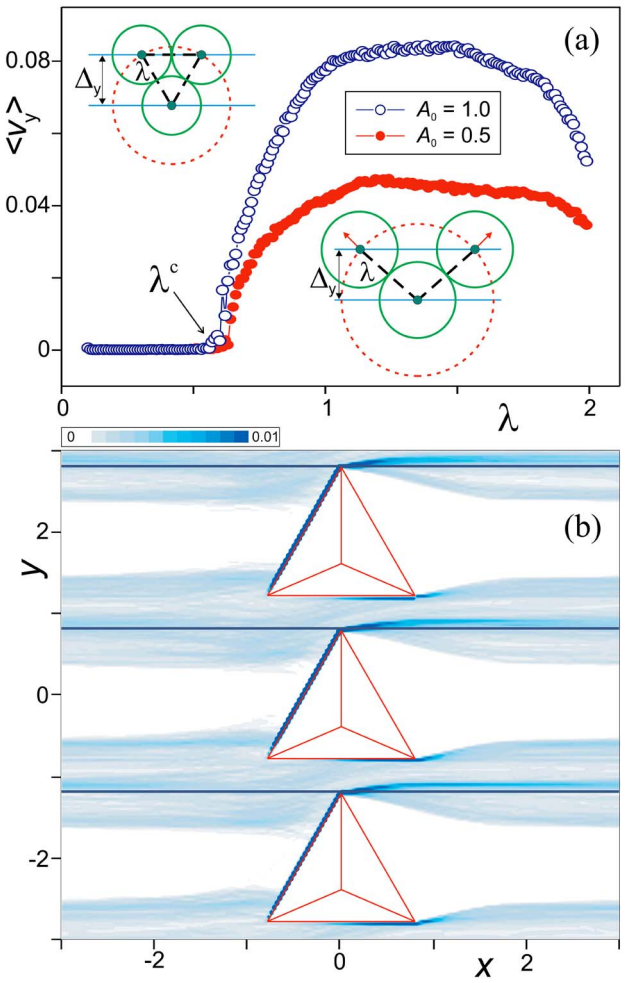

FIG. 6. (Color online) Dependence of $\langle V_y \rangle$ on the interaction length λ for particles moving through an array of 2D potential energy pyramids ($a_y=2, a_x=6$, $l=0.8$, $\Delta_x=4.4$, $\Delta_y=0.4$, $q=1$, $g=0.1$). The existence of a threshold value λ^c, see text, is apparent. Upper (lower) inset schematically shows a dense (dilute) packing of particles and the corresponding relations between λ_c and Δ_y. Contour plots of the corresponding particle distributions are shown in (b): short-range interacting particles move along straight lines, while long-range interacting particles spread out providing transverse motion.

ticles is rectified into the y direction. This regime applies for increasing A_0 until particles start crossing over the (tip of the) triangle [see Figs. 5(c) and 5(e)].

Despite of these similarities, the particle distribution in the case of long-range interaction is clearly reminiscent of an underlying triangular lattice structure [Figs. 5(b) and 5(c)] at low drives: therefore, for $A \ll q/l$ the particle motion occurs in the form of "jumps" between equilibrium lattice configurations [Fig. 5(b)], as the particles are arranged according to a triangular lattice distorted by the triangular obstacles; for higher A_0, particle motion follows closed trajectories [Fig. 5(c)]. In contrast, weak short-range interactions split the particle flow into parallel streams [Fig. 4(d)] along the edge of the pyramids for $A_0 \lesssim q/l$ [rising branch of $\langle V_y(A_0) \rangle$], while for strong drives $A_0 \gtrsim q/l$ [decaying branch of $\langle V_y(A_0) \rangle$] the particles run across the triangles, altogether [Fig. 5(e)]. At nonzero temperatures the curves $\langle V_y(A_0) \rangle$ become less and less sensitive to the interaction constant g.

Particle separation according to their interaction length

For the case of a 2D array of pyramids with $q>0$, a gap between triangles along the y axis, $\Delta_y>0$, makes the net current sensitive to the interaction length λ (Fig. 6). Namely, if the interparticle interaction length is smaller than a certain threshold value

$$\lambda < \lambda^c \sim \Delta_y, \tag{5}$$

then the net current turns out to be zero. If λ exceeds λ^c then the current rapidly increases. Note that the threshold value λ^c depends on the particle density. At high densities, particles

form a tight (triangular) packing [see upper inset to Fig. 6(a)]. The obvious geometrical consideration results in

$$\lambda^c = \frac{2\sqrt{3}}{3}\Delta_y ,$$

for large density. When the particle density decreases, the particle packing becomes more and more diluted [lower inset to Fig. 6(a)] resulting in a monotonic decay of the threshold value λ^c. In the low-density limit, we obtain

$$\lambda^c(n \to 0) = 0.$$

This effect could be used to separate particles according to their interaction length. More precisely, particles having an interaction length smaller than λ^c would pass through the array, or sieve of obstacles separated by Δ_y. In contrast, particles with a longer interaction length $\lambda > \lambda^c$ would be sifted sidewise. On connecting several such sieves with different gap Δ_y, one can construct a device capable of separating the different fractions of a particle mixture. Examples of particle species with different interaction lengths, which could be subject to our separation technique, include different ions (e.g., either positive or negative) or particles with different magnetic moments, among others. Namely, particles with very different values of the electrical charge (or magnetic moment).

VI. CONCLUSIONS

We have studied how inertia and particle pair interactions can induce transverse rectification of particle flows driven through square arrays or chains of triangular defects perpendicularly to their symmetry axis (i.e., their reflection axis). Our main results can be summarized as follows.

• Thermal noise assists transverse rectification of nonmassive, noninteracting particles, as they diffuse perpendicularly to the driving force, across adjacent triangle rows. The corresponding transverse net current exhibits a maximum as a function of temperature and drive amplitude, whereas it decays monotonically with the drive frequency.

• Inertia affects transverse rectification in many ways. For potential hills (obstacles), the particle motion occurs along periodic attractors; the inertia-induced transverse net current shows narrow rectification windows when increasing the driving force. We have shown that thermal fluctuations interfere with inertia, causing a broadening of the rectification windows. For potential wells (pins), particle motion is shown to be very irregular (chaotic). A sharp onset of the rectification mechanism has been detected for a certain drive amplitude; on further increasing the drive amplitude the transverse current stays constant and then decays smoothly to zero.

• For overdamped interacting particles, we have described a transverse rectification in the presence of both weak short-range and strong long-range inter-particle forces. Even though the dependence of the rectification currents on the drive amplitude is similar in the two cases, the particle motion is qualitatively different. In particular, at low drive, for strong long-range interactions the particle motion occurs in the form of jumps between equilibrium lattice configurations; in contrast, weak short-range interacting particles sustain weakly correlated rectified flows.

The net current exhibits a sharp onset threshold as a function of the interaction length. This effect can provide an additional tool for controlling the motion of tiny objects, e.g., for separating different species of a mixture of particles. For microparticles and nanoparticles, there are not that many effective separation techniques. This has motivated many groups to work along this direction; see, e.g., Refs. 29–38. Thus, our studies could be used either to improve or to develop potentially useful separation techniques.

ACKNOWLEDGMENTS

This work was supported in part by the National Security Agency (NSA) and Advanced Research and Development Activity (ARDA) under Air Force Office of Scientific Research (AFOSR) Contract No. F49620-02-1-0334, and also supported by the US National Science Foundation Grant No. EIA-0130383, and RIKEN's President's funds.

APPENDIX A: ANALYTICAL ESTIMATION OF THE TRANSVERSE VELOCITY OF DIFFUSING OVERDAMPED PARTICLES

In order to estimate the net transverse velocity of overdamped particles driven by a dc force A_0 with $T>0$, we start calculating the approximate time τ_{AD} a particle takes to move from point A to point D in the geometry of Fig. 1(b). Since the distance between A and B is $l\sqrt{5}$ and the component of the driving force on the A-B direction is $A_0/\sqrt{5}$, the average time τ_{AB} a particle spends along the triangle side AB is

$$\tau_{AB} \approx \frac{5l\eta}{A_0}.$$

It takes a time

$$\tau_{BD} \approx \frac{(a_x - l)\eta}{A_0}$$

to get from B to D. Therefore, for particles diffusing to the next row of triangles, the transverse average velocity $\tilde{V}$ would be

$$\tilde{V} = \frac{a_y}{\tau_{AB} + \tau_{BD}}.$$

In order to estimate the net transverse velocity

$$\langle V_y \rangle = P_{\text{diff}}\tilde{V},$$

we need to determine the probability, P_{diff}, of particle diffusion across two adjacent rows of triangles in the absence of bias. We assume that the particle is free to diffuse in the y direction between point B with $y=0$ and the reflecting wall at $y=\Delta_y$, representing the base of the opposite triangle, with distribution density

$$P_{BC}(y,t) = \frac{1}{\sqrt{4\pi Tt/\eta}}\left\{\exp\left(-\frac{ny^2}{4Tt}\right) + \exp\left(-\frac{n(y-2\Delta_y)^2}{4Tt}\right)\right\}. \quad \text{(A1)}$$

The particle motion in the x direction is assumed to be fluctuationless with steady velocity A_0/η. Therefore, after reaching the "corner C" of the lane crossing at time $t_1=\eta l/A_0$, the particle can then move vertically farther past points C and D [no reflecting wall, see Fig. 1(b)]. Thus, the particle distribution beyond point C can be approximated to

$$P_{CD}(y,t) = \int_{-\infty}^{\Delta_y} dy'\, P_{BC}(y',t_1)\frac{\exp[-\eta(y-y')^2)/(4T\tau)}{\sqrt{4\pi T\tau/\eta}} \quad \text{(A2)}$$

with $\tau=t-t_1$. Accordingly, the probability P_{diff} for the particle to diffuse across the opening CD is equal to the probability of finding the particle with $y>\Delta_y$ at time $t_2=\eta(a_x-l)/A_0$, i.e.,

$$P_{\text{diff}} = \int_{\Delta_y}^{\infty} dy\, P_{CD}(y,t_2). \quad \text{(A3)}$$

After some simple algebra we obtain the approximate expression (4) for the net transverse velocity. Note that particle diffusion through openings on the right-hand side (rhs) of point E in Fig. 1(b) has been ignored in Eq. (4). The diffusion through other openings can be roughly taken into account using the following expression:

$$\langle V_y\rangle = \sum_{n=0}^{\infty} \frac{a_y}{\tau_{AB}+\tau_{BD}+na_x\eta/A_0} P_{\text{diff}}(1-P_{\text{diff}})^n. \quad \text{(A4)}$$

Using Eq. (A4) provides a better fit to our simulation data [see Fig. 2(c) green dashed curve].

APPENDIX B: TRANSVERSE MOTION OF EXTREMELY UNDERDAMPED PARTICLES

Here we present simulation data for particles with very large inertia, $a_x \ll qm/(\eta^2 l)$. In this case, a nonzero transverse velocity (either positive or negative) was found only for dc drives and zero temperature [see Fig. 7(a)]. The corresponding trajectories are almost straight lines [Figs. 7(b) and 7(c)] because inertia is so large that only multiple collisions with the potential hills can deviate particles from the x direction. In order to understand the origin of such trajectories we had recourse to the "reduced zone" scheme shown in the inset of Fig. 7(d): Trajectories are folded on one lattice cell, say, the cell $U(x,y)$ of Eq. (1) with $k_x=k_y=0$; regular trajectories will cross the symmetry axis $x=0$ of the reduced cell N times (i.e., the winding number defined in Sec. IV); the dynamical effects of the particle-barrier collisions are to be reproduced by an *ad hoc* periodic effective potential $U(y)$,

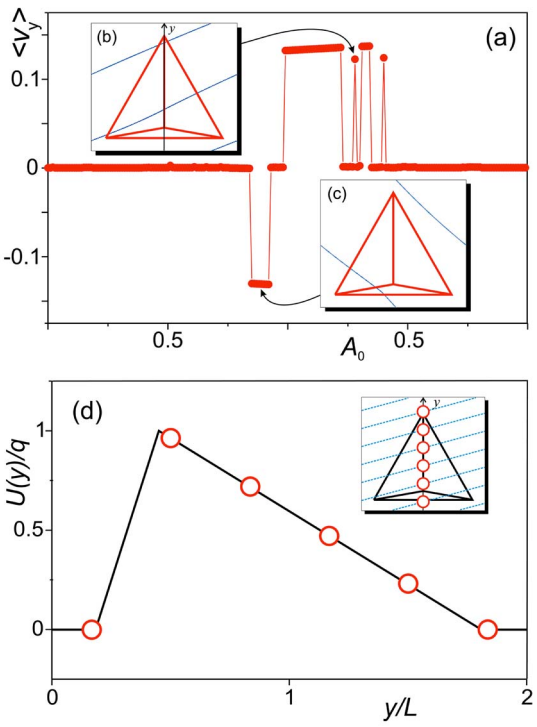

FIG. 7. (Color online) (a) Transverse motion of extremely underdamped particles driven by a dc force A_0 at zero temperature: $m=111$, $\eta=2$, $a_x=2$, $a_y=2$, $l=0.8$, $l_0=0.1$, $q=1$, $\Delta_x=0.4$, and $\Delta_y=0.4$. Particle distributions shown in (b), (c) correspond to the A_0 values marked by arrows in (a). Panel (d) shows an example of collisional map (see text) for a trajectory with winding number $N=6$.

with y denoting the point on the cell symmetry axis where the particle crosses the barrier, i.e., $U(y)=U(x=0,y)$. For the argument that follows, the exact shape of $U(y)$ is immaterial. As such a point (or "particle") on this 1D map moves continuously along the y-axis subject to a 1D periodic potential, $U(y)=U(y+L)$, it experiences a null average force $\langle U'(y)\rangle$:

$$\left\langle \frac{dU(y)}{dy} \right\rangle = \langle U'(x)\rangle = \frac{1}{L}\int_0^L U'(y)dy.$$

Correspondingly, for a particle crossing a triangular pyramid randomly along its symmetry axis, no net transverse drift is expected, namely $\langle V_y\rangle=0$. Closed trajectories with winding number N [Figs. 7(b) and 7(c)] occur when the particle enters the triangles through N fixed points [open circles in Fig. 7(d)]. This produces an effective force

$$\langle U'(y)\rangle = \frac{1}{N}\sum_1^N U'(y_i) \neq 0$$

that generates the transverse component of the particle motion.

[1] For reviews, see the special issues: *Ratchets and Brownian Motors: Basics, Experiments and Applications*, edited by H. Linke, Appl. Phys. A: Mater. Sci. Process. 75 (2002) and; *Transport in Molecular Wires*, edited by P. Hänggi, M. Ratner, and S. Yaliraki, Chem. Phys. 281 (2002).

[2] See, e.g., the reviews: P. Reimann, Phys. Rep. **361**, 57 (2002); R. D. Astumian and P. Hänggi, Phys. Today **55**, 33 (2002); F. Jülicher, A. Ajdari, and J. Prost, Rev. Mod. Phys. **69**, 1269 (1997); R. D. Astumian, Science **276**, 917 (1997); P. Hänggi, F. Marchesoni, and F. Nori, Ann. Phys. (Leipzig) **14**, 51 (2005).

[3] S. Matthias and F. Müller, Nature (London) **424**, 53 (2003).

[4] Z. Siwy and A. Fuliński, Phys. Rev. Lett. **89**, 198103 (2002); C. Marquet, A. Buguin, L. Talini, and P. Silberzan, *ibid.* **88**, 168301 (2002).

[5] L. R. Huang, E. C Cox, R. H. Austin, and J. C. Sturm, Anal. Chem. **75**, 6963 (2003).

[6] R. Austin, Nat. Mater. **2**, 567 (2003).

[7] P. T. Korda, M. B. Taylor, and D. G. Grier, Phys. Rev. Lett. **89**, 128301 (2002); B. A. Koss and D. G. Grier, Appl. Phys. Lett. **82**, 3985 (2003).

[8] E. R. Dufresne, D. Altman, and D. G. Grier, Europhys. Lett. **53**, 264 (2001); E. R. Dufresne, T. M. Squires, M. P. Brenner, and D. G. Grier, Phys. Rev. Lett. **85**, 3317 (2000).

[9] P. T. Korda and D. G. Grier, J. Chem. Phys. **114**, 7570 (2001).

[10] P. T. Korda, G. C. Spalding, and D. G. Grier, Phys. Rev. B **66**, 024504 (2002).

[11] D. G. Grier, Nature (London) **424**, 810 (2003).

[12] J. E. Villegas, S. Savel'ev, F. Nori, E. M. Gonzalez, J. V. Anguita, R. García, and J. L. Vicent, Science **302**, 1188 (2003).

[13] R. Wördenweber, P. Dymashevski, and V. R. Misko, Phys. Rev. B **69**, 184504 (2004).

[14] A. M. Song, A. Lorke, A. Kriele, J. P. Kotthaus, W. Wegscheider, and M. Bichler, Phys. Rev. Lett. **80**, 3831 (1998).

[15] A. M. Song, P. Omling, L. Samuelson, W. Seifert, I. Shorubalko, and H. Zirath, Appl. Phys. Lett. **79**, 1357 (2001).

[16] B. Y. Zhu, F. Marchesoni, V. V. Moshchalkov, and F. Nori, Phys. Rev. B **68**, 014514 (2003); Physica C **388–389**, 665 (2003); **404**, 260 (2004); F. Marchesoni, B. Y. Zhu, and F. Nori, Physica A **325**, 78 (2003).

[17] A. Gopinathan and D. G. Grier, Phys. Rev. Lett. **92**, 130602 (2004).

[18] D. A. Doyle, J. M. Cabral, R. A. Pfuetzner, A. Kuo, J. M. Gulbis, S. L. Cohen, B. T. Chait, and R. MacKinnon, Science **280**, 69 (1998).

[19] R. D. Astumian, Phys. Rev. Lett. **91**, 118102 (2003).

[20] Here we assume the particles to be small enough such that their energy is of the order of the thermal fluctuation energy. This can apply to, e.g., colloidal particles, electrons, vortices in superconductors, micron-size, or nanoscale particles. For instance, for massive nanoparticles, comparing kinetic and thermal energies, we can obtain an estimate for the particle's size, $R \sim (k_B T/\rho V^2) \sim 100$ nm, for $T=300$ K, density $\rho = 7 \times 10^3$ kg/m^3, and velocity 0.2 mm/s.

[21] P. Jung, J. G. Kissner and P. Hänggi, Phys. Rev. Lett. **76**, 3436 (1996).

[22] J. L. Mateos, Phys. Rev. Lett. **84**, 258 (2000); M. Borromeo, G. Costantini, and F. Marchesoni, Phys. Rev. E **65**, 041110 (2002).

[23] S. Savel'ev, F. Marchesoni, P. Hänggi, and F. Nori, Europhys. Lett. **67**, 179 (2004); Eur. Phys. J. B, 066109 (2004); Phys. Rev. E **70**, 066109 (2004).

[24] S. Savel'ev and F. Nori, Nat. Mater. **1**, 179 (2002).

[25] S. Savel'ev, F. Marchesoni, and F. Nori, Phys. Rev. Lett. **91**, 010601 (2003).

[26] S. Savel'ev, F. Marchesoni, and F. Nori, Phys. Rev. Lett. **92**, 160602 (2004); Phys. Rev. E **70**, 061107 (2004); Phys. Rev. E **71**, 011107 (2005).

[27] A. Engel, H. W. Müller, P. Reimann, and A. Jung, Phys. Rev. Lett. **91**, 060602 (2003).

[28] R. Eichhorn, P. Reimann, and P. Hänggi, Phys. Rev. Lett. **88**, 190601 (2002).

[29] D. Ertas, Phys. Rev. Lett. **80**, 1548 (1998).

[30] T. A. J. Duke and R. H. Austin, Phys. Rev. Lett. **80**, 1552 (1998).

[31] I. Derényi and R. D. Astumian, Phys. Rev. E **58**, 7781 (1998).

[32] L. R. Huang, P. Silberzan, J. O. Tegenfeldt, E. C. Cox, J. C. Sturm, R. H. Austin, and H. Craighead, Phys. Rev. Lett. **89**, 178301 (2002);

[33] L. R. Huang, J. O. Tegenfeldt, J. J. Kraeft, J. C. Sturm, R. H. Austin, and E. C. Cox, Nat. Biotechnol. **20**, 1048 (2002).

[34] O. Bakajin, T. A. J. Duke, J. Tegenfeldt, C. F. Chou, S. S. Chan, R. H. Austin, and E. C. Cox, Anal. Chem. **73**, 6053 (2001).

[35] M. Berger, J. Castelino, R. Huang, M. Shah, and R. H. Austin, Electrophoresis **22**, 3883 (2001).

[36] A. Oudenaarden and S. G. Boxer, Science **285**, 1046 (1999).

[37] L. R. Huang, E. C. Cox, R. H. Austin, and J. C. Sturm, Science **304**, 987 (2004).

[38] M. Bier, M. Kostur, I. Derényi, and R. D. Astumian, Phys. Rev. E **61**, 7184 (2000).

[39] J. F. Wambaugh, C. Reichhardt, C. J. Olson, F. Marchesoni, and F. Nori, Phys. Rev. Lett. **83**, 5106 (1999). This work uses triangular pinning to rectify ac-driven vortices.

[40] C. Keller, F. Marquardt, and C. Bruder, Phys. Rev. E **65**, 041927 (2002).

[41] B. Y. Zhu, F. Marchesoni, and F. Nori, Phys. Rev. Lett. **92**, 180602 (2004); Physica E (Amsterdam) **18**, 318 (2003).

[42] B. Y. Zhu, L. Van Look, F. Marchesoni, V. V. Moshchalkov, and F. Nori, Physica E (Amsterdam) **18**, 322 (2003).

[43] The potential energy of each trap has the shape of an "elongated tetrahedron," hereafter denoted by the word "pyramid."

[44] J. Van de Vondel, C. C. de Souza Silva, B. Y. Zhu, M. Morelle, and V. V. Moshchalkov, Phys. Rev. Lett. **94**, 057003 (2005).